Supporting Information for: Impact of Vibrational Modes in the Plasmonic Purcell Effect of Organic Molecules

Dongxing Zhao,[†,‡] Rui E. F. Silva,[‡] Clàudia Climent,[‡] Johannes Feist,[‡] Antonio I. Fernández-Domínguez,[‡] and Francisco J. García-Vidal[*,‡,¶]

†*School of Physical Science and Technology, Southwest University, Chongqing 400715, China*

‡*Departamento de Física Teórica de la Materia Condensada and Condensed Matter Physics Center (IFIMAC), Universidad Autónoma de Madrid, E-28049 Madrid, Spain*

¶*Donostia International Physics Center (DIPC), E-20018 Donostia/San Sebastián, Spain*

E-mail: fj.garcia@uam.es

1 Model

We first consider a two-level system (TLS) in a complex electromagnetic (EM) environment. According to the macroscopic quantum electrodynamics formalism,[S1,S2] the Hamiltonian of a TLS embedded in a dispersing and absorbing media could be written as

$$\begin{aligned} H &= \hbar\omega_e\sigma_+\sigma_- + \int d\omega \int d^3\mathbf{r}\hbar\omega\mathbf{f}^\dagger(\mathbf{r},\omega)\cdot\mathbf{f}(\mathbf{r},\omega) \\ &\quad - \int d\omega(\sigma_+ + \sigma_-)\boldsymbol{\mu}\cdot\left[\mathbf{E}^{(+)}(\mathbf{r}_e,\omega) + \mathbf{E}^{(-)}(\mathbf{r}_e,\omega)\right], \end{aligned} \tag{S1}$$

with the (positive-frequency) EM field $\mathbf{E}^{+}(\mathbf{r}_e,\omega)$ at TLS position $\mathbf{r}_e$ given by

$$\mathbf{E}^{(+)}(\mathbf{r}_e,\omega)=\int d^3\mathbf{r}' i\frac{\omega^2}{c^2}\sqrt{\frac{\hbar}{\pi\varepsilon_0}\mathrm{Im}\varepsilon(\mathbf{r}',\omega)}\mathbf{G}(\mathbf{r}_e,\mathbf{r}',\omega)\cdot\mathbf{f}(\mathbf{r}',\omega), \tag{S2}$$

where the $\mathbf{G}(\mathbf{r}_e,\mathbf{r}',\omega)$ is the classical Green's tensor, $\varepsilon(\mathbf{r}',\omega)$ is the relative electric permittivity of EM environment, and $\mathbf{f}(\mathbf{r}',\omega)$ is the annihilation operator of bosonic excitation with frequency ω at position $\mathbf{r}'$. Inspired by the form of the interaction Hamiltonian, we introduce the emitter-centered modes,[S2,S3]

$$a(\mathbf{r}_e,\omega)=-\frac{1}{\hbar g_\omega}\boldsymbol{\mu}\cdot\mathbf{E}^{(+)}(\mathbf{r}_e,\omega), \tag{S3}$$

where the prefactor

$$g_\omega=\sqrt{\frac{\mu_0\omega^2}{\pi\hbar}\boldsymbol{\mu}\cdot\mathrm{Im}\mathbf{G}(\mathbf{r}_e,\mathbf{r}_e,\omega)\cdot\boldsymbol{\mu}} \tag{S4}$$

is chosen to ensure the commutation relation $[a(\mathbf{r}_e,\omega),a^\dagger(\mathbf{r}_e,\omega')]=\delta(\omega-\omega')$. In the following the $a(\mathbf{r}_e,\omega)$ is denoted by a_ω for simplicity. Inserting the Eq. (S3) to Eq. (S1) gives

$$H=\hbar\omega_e\sigma_+\sigma_-+\int d\omega\left[\hbar\omega a_\omega^\dagger a_\omega+\hbar g_\omega(\sigma_++\sigma_-)(a_\omega^\dagger+a_\omega)\right], \tag{S5}$$

in which the Hamiltonian related to dark modes (in the sense of being decoupled from the TLS) has been dropped.

Notice that g_ω is closely related to the Purcell enhancement $P(\omega)$ through $P(\omega)=2\pi g_\omega^2/\gamma_0$, with γ_0 being the decay rate of a TLS in free space. Therefore, by calculating the radiative and non-radiative Purcell enhancement of a TLS in a complex EM environment, one can disentangle the EM modes into two groups, radiative and non-radiative modes, denoted with operators $a_{\mathrm{r},\omega}$ (with coupling strength $g_{\mathrm{r},\omega}$) and $a_{\mathrm{nr},\omega}$ (with coupling strength $g_{\mathrm{nr},\omega}$), respectively.

For organic molecules, the electronic transition also couples to the molecular vibrations. Introducing the dressing effect by these vibrational modes, and using rotating-wave approx-

imation for the excition-EM mode coupling, one finally arrives [$\hbar = 1$]

$$\begin{aligned} H \quad &= \omega_e \sigma_+ \sigma_- + \int d\omega \left[\omega b_\omega^\dagger b_\omega + \lambda_\omega \left(b_\omega^\dagger + b_\omega \right) \sigma_+ \sigma_- \right] \\ &+ \sum_{i=\mathrm{nr,r}} \int d\omega \left[\omega a_{i,\omega}^\dagger a_{i,\omega} + g_{i,\omega} \left(a_{i,\omega}^\dagger \sigma_- + a_{i,\omega} \sigma_+ \right) \right], \end{aligned} \tag{S6}$$

which is the Eq. (1) in the main text.

Given that the plasmonic environment consists of both radiative and non-radiative parts, one may guess that the decay dynamics depend on the respective values of each components. However, as shown in the following, the dynamics of the molecules are governed by the total EM spectral density $J_\mathrm{p}(\omega)$ only. To this end, starting from Eq. (S6), we first introduce two sets of new plasmonic modes

$$a_\omega = \alpha_{\mathrm{nr},\omega} a_{\mathrm{nr},\omega} + \alpha_{\mathrm{r},\omega} a_{\mathrm{r},\omega}, \tag{S7}$$

$$d_\omega = \alpha_{\mathrm{r},\omega} a_{\mathrm{nr},\omega} - \alpha_{\mathrm{nr},\omega} a_{\mathrm{r},\omega}, \tag{S8}$$

where the coefficients $\alpha_{i,\omega}$ are defined by $\alpha_{i,\omega} = g_{i,\omega}/g_\omega$, with $g_\omega = \sqrt{g_{\mathrm{nr},\omega}^2 + g_{\mathrm{r},\omega}^2}$. Rewriting Eq. (S6) with the new operators gives

$$\begin{aligned} H \quad &= \omega_e \sigma_+ \sigma_- + \int d\omega \left[\omega b_\omega^\dagger b_\omega + \lambda_\omega \left(b_\omega^\dagger + b_\omega \right) \sigma_+ \sigma_- \right] \\ &+ \int d\omega \left[\omega a_\omega^\dagger a_\omega + \omega d_\omega^\dagger d_\omega + g_\omega \left(a_\omega^\dagger \sigma_- + a_\omega \sigma_+ \right) \right]. \end{aligned} \tag{S9}$$

Here one can see that d_ω acts as a *dark* mode that is decoupled from the exciton. Moreover, the original EM modes can be expressed in terms of the new mode operators as

$$a_{\mathrm{nr},\omega} = \alpha_{\mathrm{nr},\omega} a_\omega + \alpha_{\mathrm{r},\omega} d_\omega, \tag{S10}$$

$$a_{\mathrm{r},\omega} = \alpha_{\mathrm{r},\omega} a_\omega - \alpha_{\mathrm{nr},\omega} d_\omega. \tag{S11}$$

Taking the non-radiative component as an example, the population in this branch can be

calculated from

$$\begin{aligned}\langle a^{\dagger}_{\mathrm{nr},\omega} a_{\mathrm{nr},\omega}\rangle &= \alpha^2_{\mathrm{nr},\omega}\langle a^{\dagger}_{\omega} a_{\omega}\rangle + \alpha^2_{\mathrm{r},\omega}\langle d^{\dagger}_{\omega} d_{\omega}\rangle \\ &\quad + \alpha_{\mathrm{nr},\omega}\alpha_{\mathrm{r},\omega}(\langle a^{\dagger}_{\omega} d_{\omega}\rangle + \langle a_{\omega} d^{\dagger}_{\omega}\rangle). \end{aligned} \tag{S12}$$

Since we assume an initial vacuum state for the EM modes and mode d_ω is decoupled from the exciton, any expectation value related with d_ω vanishes. With this argument we arrive to the following expression for both the radiative and non-radiative components,

$$\langle a^{\dagger}_{i,\omega} a_{i,\omega}\rangle = \alpha^2_{i,\omega}\langle a^{\dagger}_{\omega} a_{\omega}\rangle = \frac{J_i(\omega)}{J_{\mathrm{p}}(\omega)}\langle a^{\dagger}_{\omega} a_{\omega}\rangle, \tag{S13}$$

with the spectral density $J_i(\omega) = g^2_{i,\omega}$ and $J_{\mathrm{p}}(\omega) = g^2_{\omega} = J_{\mathrm{nr}}(\omega) + J_{\mathrm{r}}(\omega)$. Therefore, the excited-state dynamics of the molecules depends only on the a_ω operators with coupling strength g_ω, and hence the total EM spectral density $J_{\mathrm{p}}(\omega)$.

2 Tensor network calculations

For convenience of tensor network calculations and the following discussion, we first rewrite the system Hamiltonian into a discrete form

$$\begin{aligned} H_{\mathrm{d}} &= \omega_e \sigma_+\sigma_- + \sum_{k=1}^{K}\left[\omega^{\mathrm{v}}_k b^{\dagger}_k b_k + \lambda_k\left(b^{\dagger}_k + b_k\right)\sigma_+\sigma_-\right] \\ &\quad + \sum_{l=1}^{L}\left[\omega^{\mathrm{p}}_l a^{\dagger}_l a_l + g_l\left(a^{\dagger}_l\sigma_- + a_l\sigma_+\right)\right], \end{aligned} \tag{S14}$$

where we have omitted the d_ω operators for simplicity. Here K and L denote numbers of discrete vibrational and plasmonic modes used to describe two continua in the system's Hamiltonian. Note that after the discretization, b_k and a_l are dimensionless operators, while λ_k and g_l have the same dimension as frequency. The spectra $S_{\mathrm{em}}(\omega) = \langle a^{\dagger}_{\omega} a_{\omega}\rangle$ defined in the main text can be obtained from $S_{\mathrm{em}}(\omega) = \langle a^{\dagger}_{l} a_{l}\rangle/\Delta\omega$, with $\Delta\omega$ being the frequency interval

for the discretization.

To enable the treatment of Eq. (S14) by the TN approach,[S4] a crucial step is applying a chain mapping transformation. It transforms the Hamiltonian into a form containing one-dimensional chains with only nearest-neighbor interactions.[S5,S6] By doing so the system Hamiltonian can be written in an equivalent chain form

$$\begin{aligned} H_{\rm c} &= \omega_e \sigma_+\sigma_- \\ &+ \sum_{k=1}^{K'} \tilde{\omega}_k^{\rm v} \tilde{b}_k^\dagger \tilde{b}_k + t_1^{\rm v}(\tilde{b}_1^\dagger + \tilde{b}_1)\sigma_+\sigma_- + \sum_{k=2}^{K'} t_k^{\rm v}(\tilde{b}_{k-1}^\dagger \tilde{b}_k + {\rm H.c.}) \\ &+ \sum_{l=1}^{L'} \tilde{\omega}_l^{\rm p} \tilde{a}_l^\dagger \tilde{a}_l + t_1^{\rm p}(\tilde{a}_1^\dagger \sigma_- + \tilde{a}_1 \sigma_+) + \sum_{l=2}^{L'} t_l^{\rm p}(\tilde{a}_{l-1}^\dagger \tilde{a}_l + {\rm H.c.}), \end{aligned} \tag{S15}$$

where $\tilde{\omega}_k^{\rm v}$ and $\tilde{b}_k$ ($\tilde{\omega}_l^{\rm p}$ and $\tilde{a}_l$) are the frequency and annihilation operator respectively for the k-th (l-th) site in the vibrational (plasmonic) chain. For $k > 1$ ($l > 1$), $t_k^{\rm v}$ ($t_l^{\rm p}$) describes the hopping strength between $(k-1)$-th and k-th ($(l-1)$-th and l-th) sites. Therefore, the exciton is now coupled to the vibrational and plasmonic chains. The former accounts for the dressing of the exciton by the molecular vibrations, while the latter leads to the exciton decay. Among many other chain parameters, $\tilde{\omega}_1^{\rm v}$, $t_1^{\rm v}$ and $t_2^{\rm v}$, denoted by $\omega_{\rm RC}$, $\lambda_{\rm RC}$ and $\gamma_{\rm d}$ respectively in the main text, are of vital importance for determining the timescales where the TLS and SVM approximations work.

The Hamiltonian in Eq. (S15) is formidable with a brute-force approach for a large number of modes. By expressing the system's wave function as a TN, i.e., a network of interconnected tensors with fewer coefficients, the computation demand can be greatly reduced.[S7] Therefore, TN methods provide an efficient way to simulate many-body dynamics and allow for the computation of a quasi-exact solution to the time-dependent Schrödinger equation for very complex systems. In this work we calculate the dynamics with the time-dependent variational matrix product states (TDVMPS) technique.[S8–S10]

The main parameters for the TN calculations in this work are as follows. For the plas-

monic part, the EM modes with frequency range from 0.6 eV to 6.0 eV have been considered, while for the molecular vibrations, all the modes of the CPDT dye have been included, lying within 0.1 to 500 meV. Both plasmonic and vibrational environment are discretized into $K = L = 6500$ modes. Nevertheless, only 650 sites [$K' = L' = 650$ in Eq. (S15)] are kept in the TN calculations, which is already enough to produce convergent results in the time range considered in the main text. One can include more chain sites, which is inevitably more computationally expensive, to extend the time range that TN calculations work. Moreover, while performing the TN calculations, a bond dimension $D = 22$ and a time step $\Delta t = 5$ a.u. have been used. All these parameters have been checked to guarantee the convergence of the results.

With regard to the organic molecule, electronic structure calculations within density functional theory and its time-dependent version were performed to obtain the vibronic coupling constants for the displaced harmonic oscillator model. The long-range corrected CAM-B3LYP functional[S11] was used together with the 6-31G(d) basis set to properly describe the charge-transfer transition. For the most stable molecular conformer of the CPDT dye,[S12] ground and excited state harmonic frequencies were calculated and the Huang-Rhys factors were obtained considering Duschinsky rotation effects.[S13] All calculations were performed with the Gaussian 16 package.[S14] Note that the CPDT dye is closely related to the commercial C218, Y123 and Dynamo Red dyes widely employed in dye sensitized solar cells.

3 Fermi's golden rule

According to the Fermi's golden rule (FGR), if a quantum emitter [transition frequency ω_0] is weakly coupled to a set of modes α [mode frequency ω_α] with a coupling strength g_α, then the irreversible decay rate of the emitter can then be calculated from

$$\gamma_0 = 2\pi \sum_\alpha g_\alpha^2 \delta(\omega_0 - \omega_\alpha). \tag{S16}$$

In the following, we apply this rule to the excited-state dynamics of the organic molecules.[S15]

Assuming that, initially, the molecule is in its electronic excited state and all plasmonic modes are in their vacuum state, one can work in the single-excitation subspace for the spontaneous emission process. Using the completeness of the vibrational basis, the Hamiltonian in Eq. (S14) can be rewritten as

$$\begin{aligned} H_{\rm d} &= \sum_{M} \omega_{e,M} |e,0,M\rangle\langle e,0,M| \\ &+ \sum_{l}\sum_{N} \omega_{g,l,N} |g,1_l,N\rangle\langle g,1_l,N| \\ &+ \sum_{l}\sum_{M,N} g_l \langle N|M\rangle (|e,0,M\rangle\langle g,1_l,N| + \text{H.c.}), \end{aligned} \tag{S17}$$

with M (N) representing a set of quantum numbers $\{m_1, m_2, \ldots, m_k, \ldots\}$ ($\{n_1, n_2, \ldots, n_k, \ldots\}$) for the vibrational basis belonging to the electronic *excited* (*ground*) state. The basis $|e,0\rangle$ ($|g,1_l\rangle$) denotes the electronic excited (ground) state, and vacuum state for all the cavity modes (one-photon state for cavity mode l and vacuum state for the remaining). Moreover, the corresponding energy for state $|e,0,M\rangle$ and $|g,1_l,N\rangle$ is $\omega_{e,M} = \omega_e - \Delta_{\rm re} + \sum_k m_k \omega_k^{\rm v}$ and $\omega_{g,l,N} = \omega_l^{\rm p} + \sum_k n_k \omega_k^{\rm v}$, respectively. The reorganization energy can be calculated as $\Delta_{\rm re} = \sum_k \lambda_k^2/\omega_k^{\rm v}$ with the discrete parameters. The spontaneous emission process is manifested through the coupling of the manifold of initial states $\{|e,0,M\rangle\}$ to the manifold of final states $\{|g,1_l,N\rangle\}$ with strength $g_l\langle N|M\rangle$. The factor $\langle N|M\rangle = \Pi_k \langle n_k|m_k\rangle$, where $\langle n_k|m_k\rangle$, known as Franck-Condon factor, is the overlap integral between the vibrational wave functions $|n_k\rangle$ and $|m_k\rangle$.

According to the FGR, if the molecule is initially in the state $|e,0,M\rangle$, then the decay rate from this state to the manifold of final states $\{|g,1_l,N\rangle\}$ reads

$$\gamma_M = 2\pi \sum_{l}\sum_{N} g_l^2 \langle M|N\rangle^2 \delta(\omega_{e,M} - \omega_{g,l,N}). \tag{S18}$$

The above equation can be written as

$$\gamma_M = 2\pi \int d\omega D_M(\omega) J_{\mathrm{p}}(\omega) \tag{S19}$$

after introducing a lineshape function $D_M(\omega)$ with

$$D_M(\omega) = \sum_N \langle M|N\rangle^2 \delta\left(\omega_{e,M} - \omega_{g,l,N} + \omega_l^{\mathrm{p}} - \omega\right) \tag{S20}$$

for a specific initial state $|e,0,M\rangle$. The corresponding *near-field emission spectra* introduced in the main text can then be calculated as

$$S_M(\omega) = \frac{2\pi}{\gamma_M}(1 - e^{-\gamma_M t}) D_M(\omega) J_{\mathrm{p}}(\omega), \tag{S21}$$

where integrating over ω yields the population in the ground state. However, the initial state of the molecule is usually a mixture of states in the manifold $\{|e,0,M\rangle\}$, with the probability of state $|e,0,M\rangle$ being $f_{e,M}$ which fulfils $\sum_M f_{e,M} = 1$. In this situation, two limiting cases are usually considered:

(i) The decay processes starting from each of the states in $\{|e,0,M\rangle\}$ are independent, which leads to a multi-exponential decay dynamics with $\langle \sigma_+ \sigma_- \rangle = \sum_M f_{e,M} e^{-\gamma_M t}$. In this case, the near-field emission spectrum $S_{\mathrm{em}}^{(i)}(\omega)$ can be obtained from

$$S_{\mathrm{em}}^{(i)}(\omega) = \sum_M f_{e,M} S_M(\omega); \tag{S22}$$

(ii) Fast phonon redistribution takes place, by thermalization for example, with a typical timescale much faster than $1/\gamma_M$. This leads to a fixed probability distribution among states $\{|e,0,M\rangle\}$ during the whole decay process. In this case, the decay of the excited-state

population is given by a single exponential as $\langle \sigma_+ \sigma_- \rangle = e^{-\gamma t}$, with the decay rate being

$$\gamma = \sum_M f_{e,M} \gamma_M. \tag{S23}$$

The above expression can also be rewritten as

$$\gamma = 2\pi \int d\omega D_{\mathrm{em}}(\omega) J_{\mathrm{p}}(\omega), \tag{S24}$$

with the averaged lineshape function $D_{\mathrm{em}}(\omega)$ given by

$$D_{\mathrm{em}}(\omega) = \sum_M f_{e,M} D_M(\omega). \tag{S25}$$

In this case, the near-field emission spectrum reads

$$S_{\mathrm{em}}^{(ii)}(\omega) = \frac{2\pi}{\gamma}(1 - e^{-\gamma t}) D_{\mathrm{em}}(\omega) J_{\mathrm{p}}(\omega). \tag{S26}$$

Strictly speaking, as we don't include any phonon redistribution mechanism in our Hamiltonian Eq. (S14), the decay should follow the multi-exponential dynamics discussed in case (i). However, as we will show below, there is no significant difference between both cases for the studied system.

To calculate the decay rate in Eqs. (S19) and (S24) and hence the lineshape function, detailed knowledge of the vibrational eigenstates and eigenenergies for both the excited and ground state potential energy surfaces is required. Here we focus on the case that the molecular vibrations can be approximately described by displaced harmonic oscillators as in Eq. (S14). With respect to the initial state, we consider a Franck-Condon excitation, the vertical transition from the vibrational ground state of the electronic ground state by

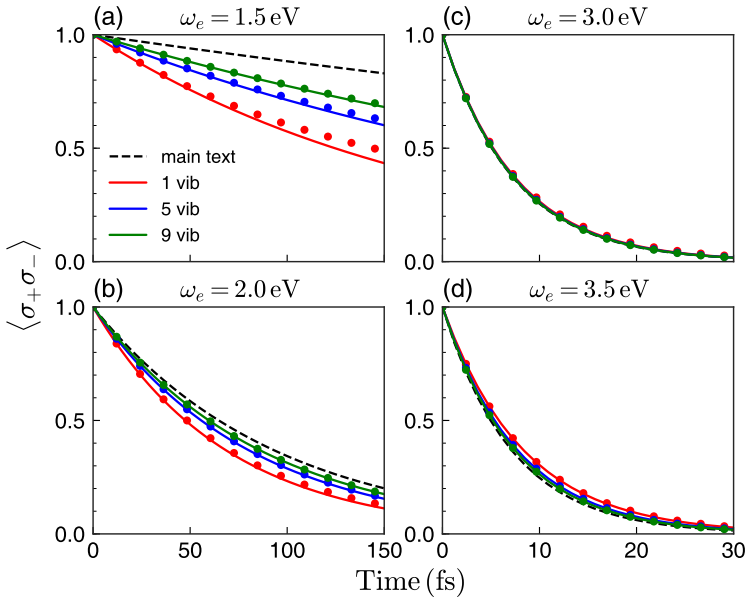

Figure S1: The excited-state dynamics $\langle \sigma_+ \sigma_- \rangle$ calculated from multi-exponential [case (*i*), dot scatters] and single-exponential dynamics [case (*ii*), solid curves] with one (red), five (blue), and nine (green) vibrational modes taken into account for the exciton frequencies discussed in the main text. The parameters for vibrational modes are obtained from an inverse chain mapping method by keeping only the first few chain sites. The FGR results considering all the vibrational modes in the main text are also shown (dashed curves).

ultrashort laser pulses. This leads to an initial distribution

$$f_{e,M} = \prod_k \frac{1}{m_k!} \left(\frac{\lambda_k}{\omega_k^{\mathrm{v}}}\right)^{2m_k} \exp\left[-\left(\frac{\lambda_k}{\omega_k^{\mathrm{v}}}\right)^2\right]. \tag{S27}$$

Now we compare the two limiting cases mentioned above. Figure S1 shows the comparison between the multi-exponential and single-exponential dynamics for an initial Franck-Condon excitation. To ease the numerical computation, only a few vibrational modes have been included. The two cases show slight differences if we consider one vibrational mode only. By increasing the number of vibrational modes, the calculations tend to converge and the differences between those two cases disappear. Moreover, due to the broadband structure and strong Purcell enhancement effect of the plasmonic pseudomode, it is easier to converge calculations for excitons coupled to this mode, meaning that the decay rates are not sensitive to the lineshape function. In contrast, the relatively narrower structure of the lower-order modes necessitate a more accurate description of the lineshape function, and hence the inclusion of more vibrational modes.

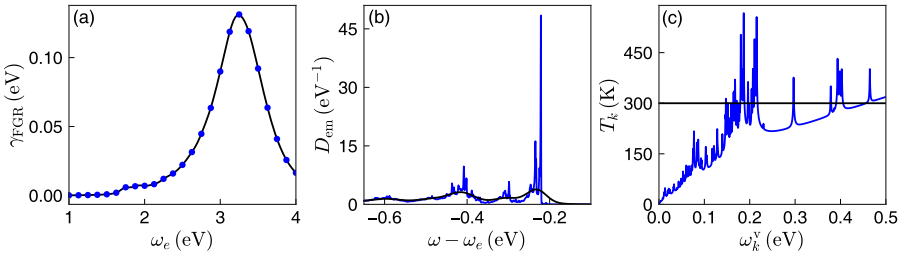

Figure S2: (a) Decay rates and (b) lineshape function calculated with the assumption of $T = 300$ K (black) and with pseudo temperatures (blue). (c) Pseudo temperatures T_k (blue) used to simulate the Franck-Condon distribution with a thermal distribution. The black horizontal line shows the temperature used for the FGR results in the main text.

Although the brute-force calculation of the lineshape function based on Eq. (S20) and (S25) works quite well for a few number of vibrational modes, they are prohibitive for hundreds of modes, which is the typical number of vibrational modes for organic molecules. Fortunately, if fast thermalization takes place for the molecular vibrations due to its interaction with a thermal reservoir at temperature T, an analytical expression for the lineshape

function can be derived as[S15]

$$D_{\rm em}(\omega) = \frac{1}{2\pi}\int dt e^{-i[\omega-(\omega_e-\Delta_{\rm re})]t-G(0)+G(t)}. \tag{S28}$$

The time-dependent function in the exponent reads

$$G(t) = \sum_k \left(\frac{\lambda_k}{\omega_k^{\rm v}}\right)^2 \{[1+n(\omega_k^{\rm v})]\, e^{-i\omega_k^{\rm v}t} + n(\omega_k^{\rm v}) e^{i\omega_k^{\rm v}t}\}, \tag{S29}$$

with $n(\omega_k^{\rm v}) = [\exp(\hbar\omega_k^{\rm v}/k_{\rm B}T)-1]^{-1}$ being the Bose–Einstein distribution function assuming a thermalized initial distribution

$$f_{e,M} = \prod_k \exp\left(-\frac{m_k\hbar\omega_k^{\rm v}}{k_{\rm B}T}\right)\left[1-\exp(-\frac{\hbar\omega_k^{\rm v}}{k_{\rm B}T})\right], \tag{S30}$$

in contrast to the Franck-Condon distribution. Interestingly, it is possible to introduce a pseudo temperature T_k for each vibrational mode k to simulate the Franck-Condon distribution with a thermal distribution, as long as the factor $\lambda_k/\omega_k^{\rm v}$ is small, say, less than 0.3. This pseudo temperature is found to be

$$k_{\rm B}T_k = -\frac{\hbar\omega_k^{\rm v}}{\ln\{1-\exp[-(\lambda_k/\omega_k^{\rm v})^2]\}}, \tag{S31}$$

which is obtained by forcing the thermal distribution to have the same vibrational ground state population as the Franck-Condon distribution.

In the main text, the lineshape function and the FGR results are based on Eqs. (S28)-(S30) with the assumption of fast thermalization at $T = 300$ K. To justify this choice, we compare the decay rates as well as the lineshape function calculated at $T = 300$ K and pseudo temperature T_k in Fig. S2. Excellent agreement for the decay rates can be found. As for the lineshape function, except for the sharp vibronic structures shown in the pseudo temperature case, the main peak positions are also in good agreement.

4 Time-dependent spectra

In Fig. 3 of the main text, we show the emission spectra evaluated at $t = 150$ fs, which could be considered as the final plasmon population after the spontaneous emission process. In this section, we show the spectra evaluated at $t = 5$ fs and $t = 75$ fs as a supplement. They show the time-dependence of the spectra obtained by different models. We point out that as the FGR approach assumes an immediate thermal redistribution, the corresponding spectra do not show any time-dependence, except for their overall intensity.

As shown in Fig. S3, the TLS spectra deviate only slightly from the TN ones at $t = 5$ fs, as the wavepacket just leaves the Frank-Condon region in this timescale. On the contrary, the SVM approximation still works in this regime, yielding spectra in good agreement with the TN results.

At longer times ($t = 75$ fs), the TLS and SVM models fail to reproduce the exact decay dynamics. As a result, they do not capture either the main feature of TN spectra, as indicated in Fig. S4. For $\omega_e = 3.0$ eV and 3.5 eV, the most of the population has already been transferred to the plasmonic dimer due to strong Purcell enhancement taking place. Therefore, the spectra calculated at 75 fs have already converged to the final spectra ($t = 150$ fs) in the main text.

References

[S1] Scheel, S.; Buhmann, S. Y. Macroscopic QED - concepts and applications. *Acta phys. Slovaca* **2008**, *58*, 675–809.

[S2] Feist, J.; Fernández-Domínguez, A. I.; García-Vidal, F. J. Macroscopic QED for quantum nanophotonics: Emitter-centered modes as a minimal basis for multi-emitter problems. *arXiv* **2020**, 2008.02106.

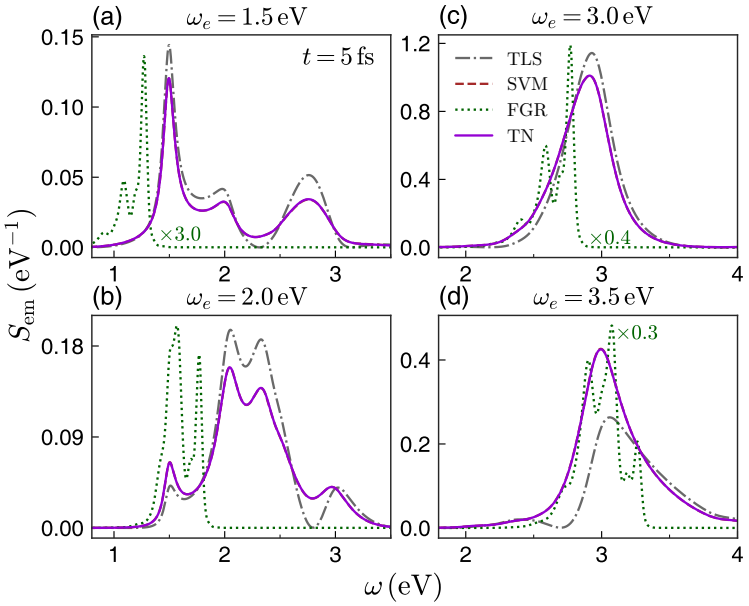

Figure S3: Near-field emission spectra $S_{\mathrm{em}}(\omega)$ for four different exciton frequencies. The spectra for the TLS and SVM approximations and full TN method are calculated at $t = 5$ fs. Note that the spectra obtained from SVM approximations overlap with TN results in this case. Some spectra have been scaled to facilitate comparison.

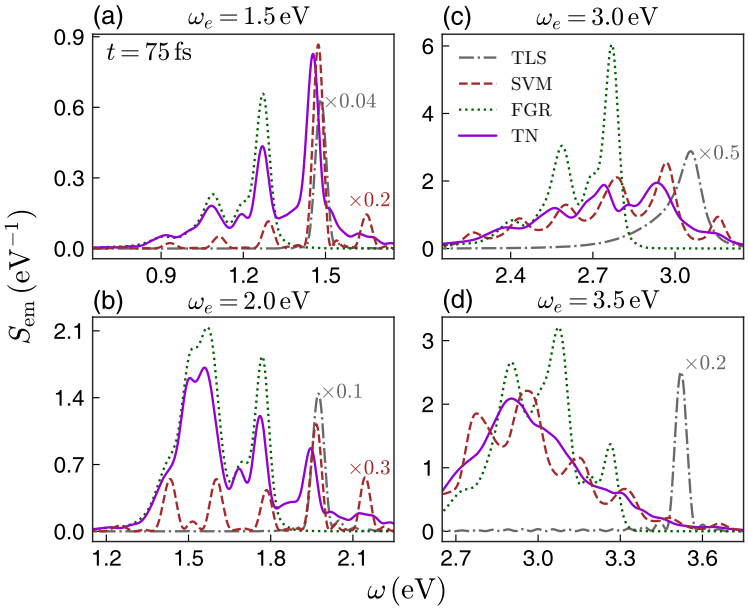

Figure S4: Same as Fig. S3 but evaluated at $t = 75$ fs.

[S3] Buhmann, S. Y.; Welsch, D.-G. Casimir-Polder forces on excited atoms in the strong atom-field coupling regime. *Phys. Rev. A* **2008**, *77*, 012110.

[S4] Schollwöck, U. The density-matrix renormalization group in the age of matrix product states. *Ann. Phys.* **2011**, *326*, 96–192.

[S5] Chin, A. W.; Rivas, Á.; Huelga, S. F.; Plenio, M. B. Exact mapping between system-reservoir quantum models and semi-infinite discrete chains using orthogonal polynomials. *J. Math. Phys.* **2010**, *51*, 092109.

[S6] Chin, A. W.; Huelga, S. F.; Plenio, M. B. *Quantum Efficiency in Complex Systems, Part II*; Semiconductors and Semimetals; Elsevier, 2011; Vol. 85; pp 115 – 143.

[S7] Orús, R. Tensor networks for complex quantum systems. *Nat. Rev. Phys.* **2019**, *1*, 538–550.

[S8] Haegeman, J.; Lubich, C.; Oseledets, I.; Vandereycken, B.; Verstraete, F. Unifying time evolution and optimization with matrix product states. *Phys. Rev. B* **2016**, *94*, 165116.

[S9] del Pino, J.; Schröder, F. A. Y. N.; Chin, A. W.; Feist, J.; Garcia-Vidal, F. J. Tensor network simulation of polaron-polaritons in organic microcavities. *Phys. Rev. B* **2018**, *98*, 165416.

[S10] Schröder, F. A.; Turban, D. H.; Musser, A. J.; Hine, N. D.; Chin, A. W. Tensor network simulation of multi-environmental open quantum dynamics via machine learning and entanglement renormalisation. *Nat. Commun.* **2019**, *10*, 1062.

[S11] Yanai, T.; Tew, D. P.; Handy, N. C. A new hybrid exchange–correlation functional using the Coulomb-attenuating method (CAM-B3LYP). *Chem. Phys. Lett.* **2004**, *393*, 51–57.

[S12] Climent, C.; Casanova, D. Electronic structure calculations for the study of D-π-A organic sensitizers: Exploring polythiophene linkers. *Chem. Phys.* **2013**, *423*, 157–166.

[S13] Duschinsky, F. The Importance of the Electron Spectrum inMulti Atomic Molecules. Concerning the Franck-Condon Principle. *Acta Physicochim. URSS* **1937**, *7*, 551.

[S14] Frisch, M. J.; Trucks, G. W.; Schlegel, H. B.; Scuseria, G. E.; Robb, M. A.; Cheeseman, J. R.; Scalmani, G.; Barone, V.; Petersson, G.; Nakatsuji, H., et al. Gaussian 16, Revision A.03. 2016.

[S15] May, V.; Kühn, O. *Charge and energy transfer dynamics in molecular systems*, 3rd ed.; WILEY-VCH Verlag GmbH & Co. KGaA: Weinheim, Germany, 2011.